Journal of Materials Science: Materials in Electronics (2019) 30:15582–15591
https://doi.org/10.1007/s10854-019-01934-5

Effects of Li_3PO_4 additive on the electrochemical properties of Li_2FeSiO_4 as cathode material for lithium-ion batteries

Ya Sun[1] · Ling Zan[1] · Youxiang Zhang[1,2]

Received: 14 January 2019 / Accepted: 25 July 2019 / Published online: 29 July 2019

Abstract
Li_2FeSiO_4/C is successfully modified by Li_3PO_4 additive to achieve excellent electrochemical properties. In comparison with bare Li_2FeSiO_4/C, the samples with Li_3PO_4 show no changes in the morphology and structure, which are verified by X-ray powder diffraction and scanning electron microscopy results. High resolution transmission electron microscopy image confirms that Li_2FeSiO_4/C and Li_3PO_4 exist in the form of nanocomposites. When used as LIB cathodes, the Li_2FeSiO_4/Li_3PO_4/C composites show notably improved electrochemical performance with outstanding high rate performance and superior cyclability than those of Li_2FeSiO_4/C. The sample with 6 mmol% (LFS-6) exhibits a large discharge capacity of 114.1 mAh g^{-1} with a remarkable capacity retention of 104.2% over 100 cycles at 10 C, which are much better than those of Li_2FeSiO_4/C (89.0 mAh g^{-1} and capacity retention of 75.9%). The enhancement in the electrochemical properties of Li_2FeSiO_4/C may be attributed to the existence of Li_3PO_4 additive with high ionic conductivity, which can accelerate the lithium ions diffusion capability and facilitate the charge transfer process.

1 Introduction

Rechargeable lithium-ion batteries (LIBs) have been highlighted for their large scale application of electronic portable devices and electric vehicles [1–3]. High capacity, high energy and power densities, low cost and lifespan are the key factors in practical applications of LIBs [4, 5]. Recently, extensive attention has been focused on lithium iron orthosilicate (Li_2FeSiO_4) because of their distinct advantages such as high security performance, obvious environmental benignity and low cost owing to the abundant resources of Fe and Si [6]. Additionally, Li_2FeSiO_4 shows high theoretical capacity (> 330 mAh g^{-1}) as a result of extracting two Li^+ ions per formula unit [7, 8]. However, like most polyanion-based cathode materials, Li_2FeSiO_4 also suffers from very low electronic conductivity ($\sim 6\times10^{-14}$ S cm^{-1}) [8, 9] together with slow lithium ion diffusion rate ($\sim 1\times10^{-14}$ cm^2 S^{-1}) [10], thus leading to extremely poor rate capability.

To solve these problems, several attempts have been made. Metal ion doping has been reported to be a suitable way to enhance the electrochemical properties of Li_2FeSiO_4 for the improved electronic conductivity and accelerated lithium ion diffusion caused by lattice defects [11–14]. Yi et al. [11] reported that Li_2FeSiO_4/C doped with 5% Mn showed excellent electrochemical performance with highest discharge capacity (248.5 mAh g^{-1} at 0.1 C) in the first cycle, outstanding high-rate performance and high value of capacity retention. Morphology control has also been illustrated to exert positive effects on the electrochemical properties of the material [15–19]. Varieties of shapes of Li_2FeSiO_4 have been investigated, such as shuttle-like [15], flower-like [16] and nanoworm-like shapes [17] as well as hollow spheres [18] and three-dimensionally ordered macroporous structure [19]. Moreover, Li_2FeSiO_4 coated with carbon has been confirmed to achieve larger discharge capacity and better cycling performance [20–22]. It is worth noting that the as-synthesized composites coated with a thin carbon layer can not only increase the electronic conductivity, but also control the particle size of material during the modification process [23, 24].

Nowadays, coating with fast ion conductor has been a widely used modified method. Various active materials such as Li_2SiO_3 [25], Fe_7SiO_{10} [26] and $AlPO_4$ [27] have been coated on the surface of Li_2FeSiO_4, which greatly improve

✉ Youxiang Zhang
yxzhang04@whu.edu.cn

[1] College of Chemistry and Molecular Sciences, Wuhan University, Wuhan 430072, China

[2] Shenzhen Research Institute of Wuhan University, Shenzhen 518000, China

the rate performance, especially the high rate performance in comparison with the original material. For instance, Li et al. [26] synthesized $Li_2FeSiO_4/Fe_7SiO_{10}/C$ via a sol–gel method by adjusting the molar ratio of Fe and Si. Compared with Li_2FeSiO_4/C, the resulting composite showed much better high-rate performance with discharge capacities of 128 and 112 mAh g^{-1}, respectively, at 5 and 10 C. As a fast lithium ion conductor, Li_3PO_4 exhibits unique advantages with ionic conductivity about 10^{-6}~10^{-8} S cm^{-1} [28, 29]. By the virtue of high ionic conductivity and strong P=O bond of Li_3PO_4, the migration rate of Li^+ between electrode and electrolyte is expected to be increased in a certain extent [30]. Importantly, Li_3PO_4 provides the possibility to reduce the corrosion of electrolyte to electrode materials when used as a coating material [31]. Hence, Li_3PO_4 has been commonly used to enhance the cyclability and rate performance of some cathodes such as $LiCoO_2$ [32], $Li(Ni_{0.4}Co_{0.3}Mn_{0.3})O_2$ [31], $LiNi_{0.5}Mn_{1.5}O_4$ [33], $LiFePO_4$ [34], $LiMn_2O_4$ [35] and Li-rich oxide [36–39].

In the present work, Li_3PO_4 has been introduced into Li_2FeSiO_4/C as a property improvement additive. The effects of different amounts of Li_3PO_4 on the structure, morphology and electrochemical performances of cathodes have been systematically investigated. By introducing Li_3PO_4, the rate performance of Li_2FeSiO_4/C can be significantly improved with nearly no capacity decay.

2 Experimental

2.1 Synthesis of Li_3PO_4

The Li_3PO_4 powder was precipitated by adding H_3PO_4 (85% solution) dropwise into 0.4 M LiOH aqueous solution with a molar ratio of Li: P equal to 3:1. The resulting white precipitates were washed with distilled water and dried at 120 °C. Finally, the Li_3PO_4 was obtained by ball-milling the dried products for 3 h.

2.2 Synthesis of Li_2FeSiO_4/C composite

Li_2FeSiO_4/C composite was prepared by a modified sol–gel method according to Ref. [40]. Firstly, 2 g poly (ethylene oxide)-b-poly (propylene oxide)-b-poly (ethylene oxide) triblock copolymer P123 (EO20PO70EO20) was dissolved in 40 mL absolute alcohol, and the stoichiometric ratio of $CH_3COOLi{\cdot}2H_2O$ and $Fe(NO_3)_3{\cdot}9H_2O$ were added into alcohol solution in order under vigorous magnetic stir. The solution was stirred and dissolved to get a uniform and transparent red-brown solution. Then the corresponding amount of TEOS was added to the mixture. The red gel was obtained under vigorous magnetic stir at 50 °C and dried at 100 °C for 12 h. Finally, the dry gel was annealed at 600 °C for 10 h under argon atmosphere. After cooling to room temperature, the products were obtained and marked as LFS.

2.3 Synthesis of $Li_2FeSiO_4/Li_3PO_4/C$ composites

The synthesized Li_3PO_4 was added into the solution containing P123, $CH_3COOLi{\cdot}2H_2O$ and $Fe(NO_3)_3{\cdot}9H_2O$ according to the given molar ratio, and the stoichiometric ratio of TEOS was dissolved in the above solution. The subsequent processing was the same as the process of Li_2FeSiO_4/C. For comparison, the molar percent of Li_3PO_4 to Li_2FeSiO_4 were 4%, 6%, 8% and 10%, respectively. The samples were marked as LFS-4, LFS-6, LFS-8 and LFS-10.

2.4 Characterization

The phase structure of as-synthesized samples was conducted by powder X-ray diffraction (Bruker D8 Advance, Germany) using Cu Kα. The morphologies and microstructures of samples were observed by scanning electron microscope (Zeiss SIGMA FESEM) and Transmission electron microscope (JEM-2100F, JEOL Ltd.). The carbon contents in the $Li_2FeSiO_4/Li_3PO_4/C$ composites and Li_2FeSiO_4/C were characterized by VARIOELIII elemental analyzer (Elementar Analysen System GmbH, Germany).

2.5 Electrochemical tests

The $Li_2FeSiO_4/Li_3PO_4/C$ composites and Li_2FeSiO_4/C, acetylene black and polytetrafluoroethylene (PTFE) binder were mixed in proportion at a ratio of 75:20:5 (in mass, wt%), and a proper amount of isopropanol was added as the dispersant. The mixture was made into paste in the mortar and transferred to the rolling machine to make film. The film was cut into disks about 1 cm in diameter and coated on stainless steel, after vacuum drying at 60 °C. In an Ar-filled glovebox, batteries were assembled using lithium foil, Celgard 2300 microporous films, 1 M $LiPF_6$ in the ethylene carbonate (EC) and dimethyl carbonate (DMC) (1:1 v/v) as anodes, separators and electrolytes, respectively. The active materials were assembled into CR2016 coin-type cell for electrochemical measurements. Galvanostatically charge–discharge tests were done between 1.5 V and 4.8 V using battery test system (Neware, China). And all the specific capacities were calculated with the mass of $Li_2FeSiO_4/Li_3PO_4/C$ composites and Li_2FeSiO_4/C, not including carbon content. Electrochemical impedance spectroscopies (EIS) were tested with an AC amplitude of 5 mV in the applied frequency of 0.01 Hz to 100 kHz via CHI760C electrochemistry workstation.

Table 1 The carbon contents in all the composites

Samples	Carbon content (wt%)
LFS	8.81
LFS-4	9.47
LFS-6	11.76
LFS-8	10.73
LFS-10	11.22

3 Results and discussion

Table 1 lists the carbon contents in $Li_2FeSiO_4/Li_3PO_4/C$ composites and Li_2FeSiO_4/C, which were characterized by elemental analyzer. Obviously, carbon contents in all the composites are very close to each other.

The XRD pattern and SEM image of the prepared Li_3PO_4 are presented in Fig. 1. Figure 1a displays that all the diffraction peaks match well with the orthogonal phase Li_3PO_4 (JCPDS NO. 71-1528). There are no impurities can be found, demonstrating that the obtained sample is pure phase. Moreover, the peak type of the sample is relatively sharp and the base is flat, suggesting the high crystallinity of the synthesized sample. From SEM image (Fig. 1b), it is clear that the particles of Li_3PO_4 after ball milling are uniform and the average diameter is about 40 nm.

Figure 2 illustrates the XRD pattern and SEM image of Li_2FeSiO_4/C. As can be seen in Fig. 2a, the reflection peaks can be assigned to the monoclinic structure Li_2FeSiO_4 with a space group of $P2_1/n$ [41]. No impurity peaks can be detected in the XRD pattern, suggesting the high purity of prepared sample. Meanwhile, no reflection peaks associated with carbon can be seen, which may be related to

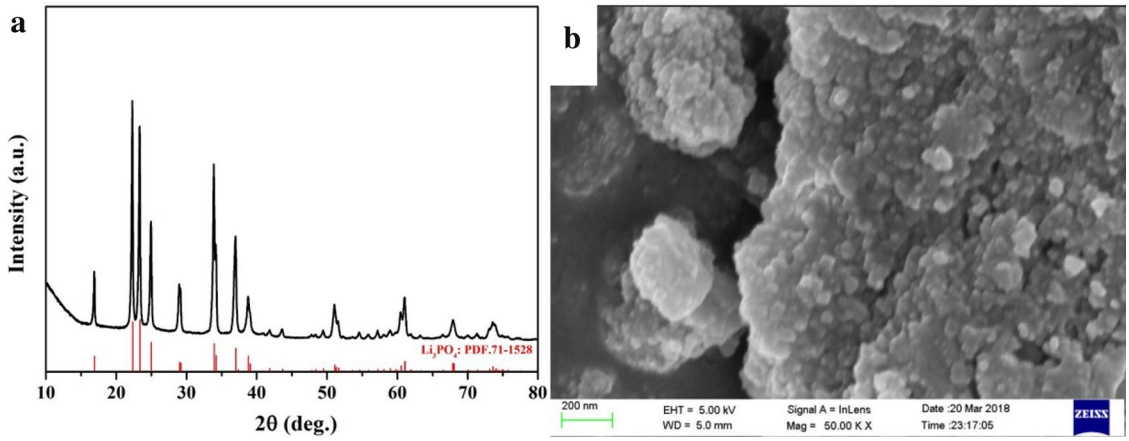

Fig. 1 The XRD pattern (**a**) and SEM image (**b**) of the prepared Li_3PO_4

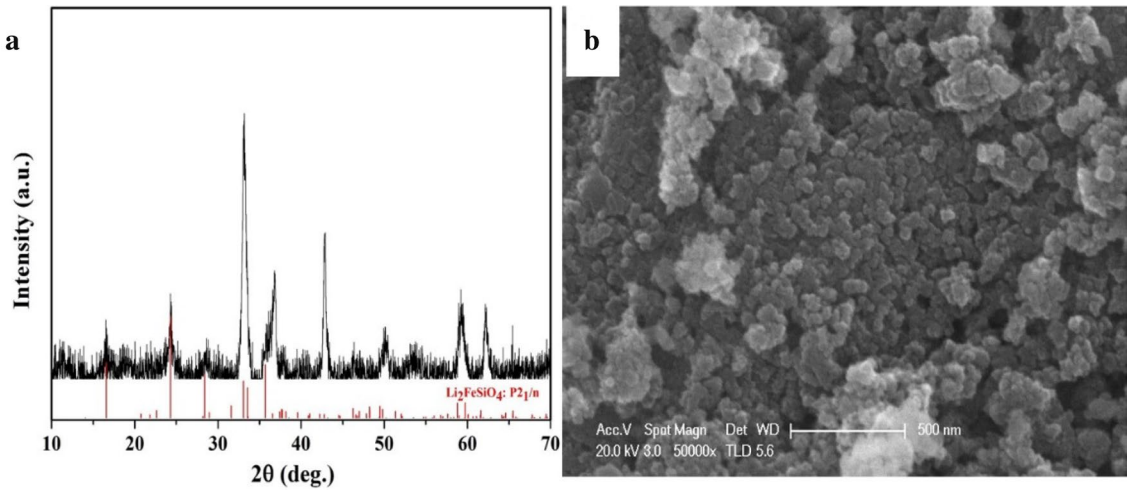

Fig. 2 The XRD pattern (**a**) and SEM image (**b**) of LFS

the amorphous property of carbon. From SEM image (In Fig. 2b), we can see that the nanoparticles are uniformly distributed and the average diameter is around 30 nm.

The XRD patterns of the samples with different contents of Li_3PO_4 (LFS-4, LFS-6, LFS-8 and LFS-10) are displayed in Fig. 3. The main reflection peaks of the samples with Li_3PO_4 are the same as those of Li_2FeSiO_4/C expect the Li_3PO_4 peaks, indicating that the crystal structure of Li_2FeSiO_4 has not been affected by Li_3PO_4. When the molar ratio of Li_3PO_4 is up to 6%, the star-labeled orthogonal phase Li_3PO_4 (JCPDS NO. 71-1528) appears in the samples. The

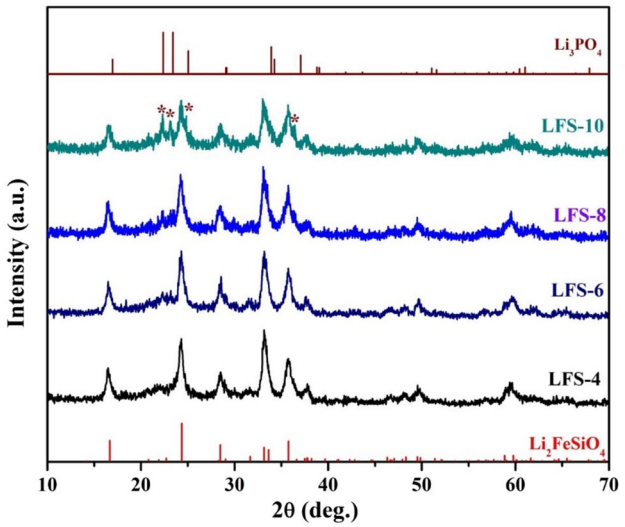

Fig. 3 The XRD patterns of the samples with different contents of Li_3PO_4 (LFS-4, LFS-6, LFS-8 and LFS-10)

diffraction peaks of Li_3PO_4 exhibit an increasing trend with enhanced amounts of Li_3PO_4. However, there are no characteristic peaks of Li_3PO_4 for LFS-4, which may be attributed to a small amount of introduced Li_3PO_4. There are also no diffraction peaks from the carbon phase shown in the patterns.

The morphologies of the samples with different contents of Li_3PO_4 were identified by SEM and the images are displayed in Fig. 4. From that, we can see the average size of nanoparticles is around 20 nm, and they are agglomerated together. The samples with different contents of Li_3PO_4 also preserve the morphology of Li_2FeSiO_4/C (Fig. 2b) with slightly decreased diameter, suggesting that Li_3PO_4 added has no effect on the morphology of Li_2FeSiO_4/C composite. To study the microstructure of LFS-6, TEM and HRTEM of material were characterized. TEM image (Fig. 5a) shows that the particles of LFS-6 are coated with amorphous carbon. From HRTEM image shown in Fig. 5b, we can clearly see the lattice fringes of Li_2FeSiO_4 and Li_3PO_4, respectively. Moreover, the interplanar spacing of 0.330 、0.235 and 0.283 nm can be well assigned to the (201), (212) and (112) facets of monoclinic Li_2FeSiO_4, while the interplanar spacing of 0.231 nm correlated well with the (021) plane of orthogonal phase Li_3PO_4. The above results suggest that Li_3PO_4 and Li_2FeSiO_4/C form nanocomposite in LFS-6.

To investigate the influences of Li_3PO_4 content on the rate performance and high-rate cyclability of Li_2FeSiO_4/C, charge–discharge experiments were performed at voltage window of 1.5–4.8 V. Figure 6a exhibits the rate performance of LFS, LFS-4, LFS-6, LFS-8 and LFS-10 at different rates from 1 C to 10 C (1 C = 166 mA g^{-1}) for 50 cycles each. It is apparently observed that Li_2FeSiO_4/C with different contents of Li_3PO_4 exhibit much better performance

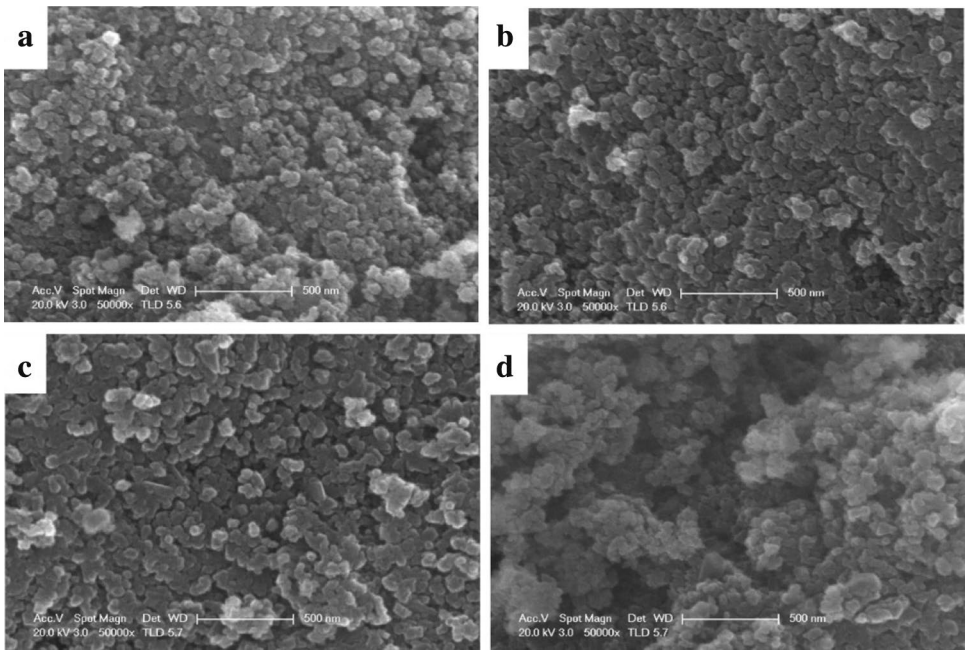

Fig. 4 SEM images of LFS-4 (**a**), LFS-6 (**b**), LFS-8 (**c**) and LFS-10 (**d**)

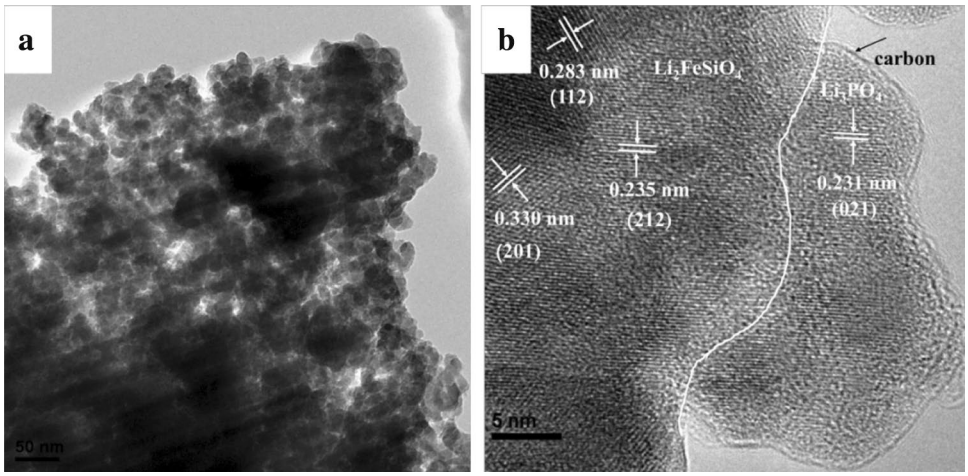

Fig. 5 TEM (**a**) and HRTEM (**b**) images of LFS-6

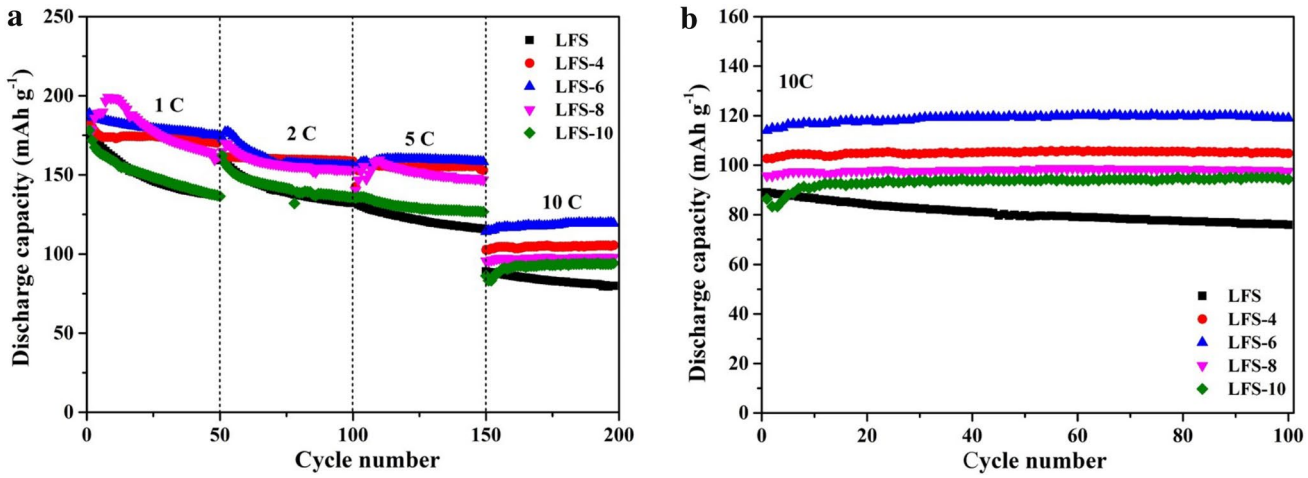

Fig. 6 Rate performance (**a**) and the cycling performance at 10 C (**b**) of LFS, LFS-4, LFS-6, LFS-8 and LFS-10

than LFS, except that LFS-10 is almost the same as that of LFS at 1 C and 2 C rates. Among the samples after adding fast ion conductor Li_3PO_4, LFS-6 possesses the best rate performance. This indicates that the introduction of Li_3PO_4 has a significant effect on improving the rate property of Li_2FeSiO_4/C, and the advantage is much more obvious on the high rate. Figure 6b presents the cycling performance of LFS, LFS-4, LFS-6, LFS-8 and LFS-10 at 10 C for 100 cycles. It is evident from the figure that the performance of LFS-6 is the best. The discharge capacity is 114.1 mAh g^{-1}, and there is no capacity decay after 100 cycles. In addition, the cyclic stability of Li_3PO_4-Li_2FeSiO_4/C composites are higher than that of LFS without Li_3PO_4.

LFS and LFS-6 were selected to further study the electrochemical performance differences between pristine sample and sample with Li_3PO_4 additive at 0.1 C at voltage window of 1.5–4.8 V. Figure 7 compares the charge–discharge curves of the two electrodes for the initial 5 cycles. Obviously, the charge–discharge curves of LFS-6 are similar to the LFS, which suggests the intrinsic properties of Li_2FeSiO_4 are not affected by Li_3PO_4. For both composites, the initial charge curves show two voltage plateaus at around 3.3 V and 4.3 V, which should be related to the Fe^{2+}/Fe^{3+} and Fe^{3+}/Fe^{4+} redox couples, respectively. However, in the subsequent charge–discharge process, the charge curves are quite different from those of the first cycle, which is attributed to structural arrangement [42]. From Fig. 7a, it can be seen the discharge capacities of LFS are 209.3, 199.4, 193.1, 186.6 and 184.8 mAh g^{-1} for the initial 5 cycles, respectively, and the capacity retention is 88.3%, while the discharge specific capacities of LFS-6 cathode material (Fig. 7b) are 195.5, 183.2, 180, 6, 179.8 and 179 mAh^{-1}, respectively, with a capacity retention of 91.8%. The LFS shows higher capacities than LFS-6 composite, however, the value of capacity retention is slightly lower than that of LFS-6. This is mainly due to the fact that Li_3PO_4 has no electrochemical activity. Although it has a negative effect on the specific capacity of

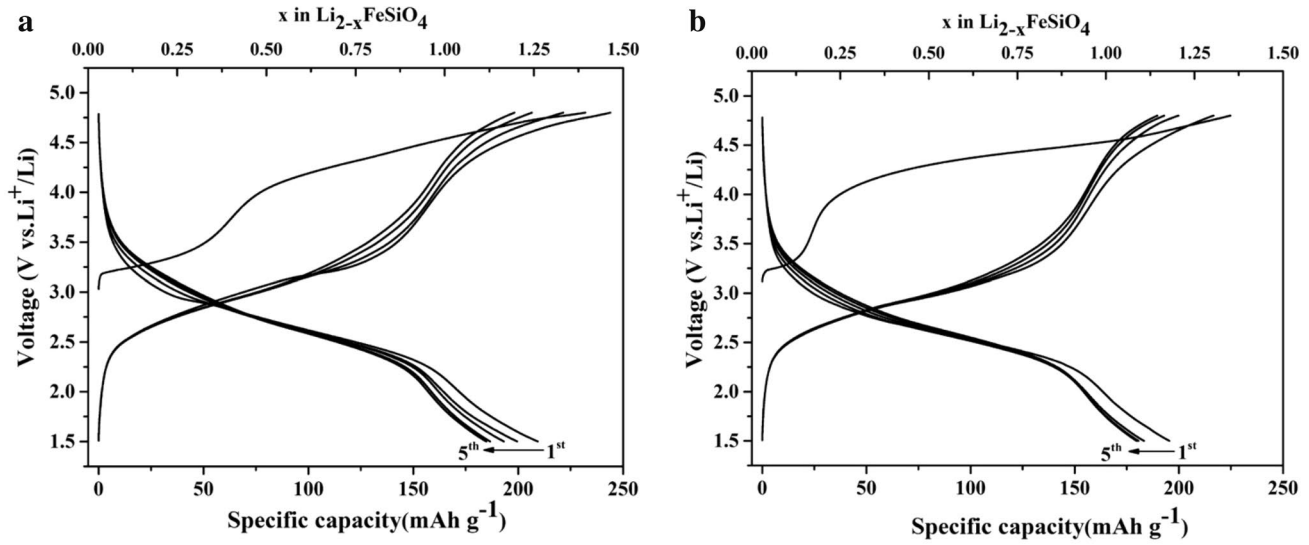

Fig. 7 The galvanostatic charge–discharge curves of LFS (**a**) and LFS-6 (**b**) at 0.1 C rate in the voltage of 1.5–4.8 V for the initial 5 cycles

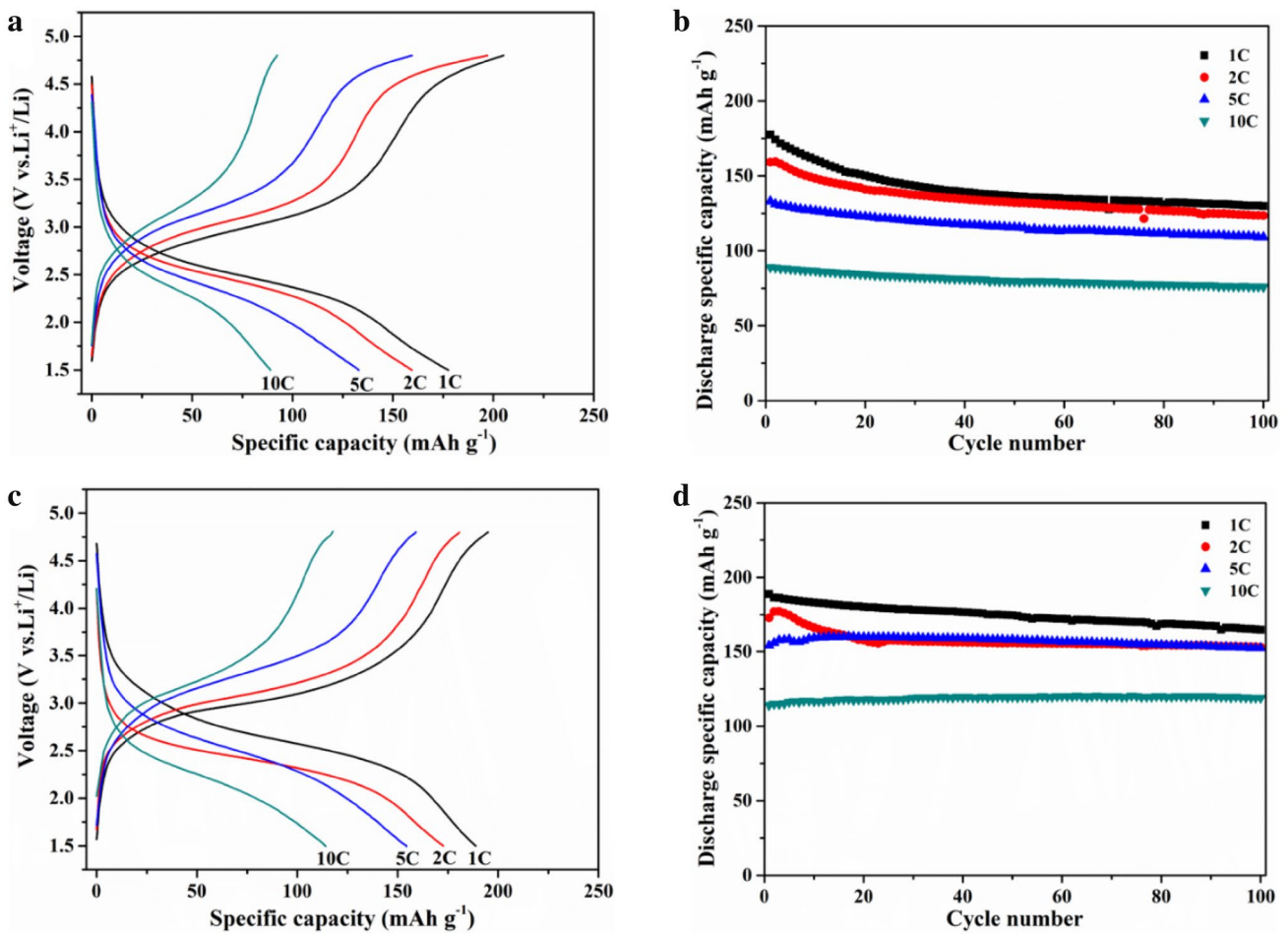

Fig. 8 The galvanostatic charge–discharge curves (**a** and **c**) and the corresponding cycling performances (**b** and **d**) of LFS and LFS-6 at rates of 1C, 2C, 5C and 10C

Table 2 Comparisons of the electrochemical performances of LFS-6 and the previous reported Li_2FeSiO_4 composites

	1C	2C	5C	10C
This work	188.8 mAh g^{-1} 87.3% (100th)	172.8 mAh g^{-1} 88.6% (100th)	154.2 mAh g^{-1} 98.8% (100th)	114.1 mAh g^{-1} 104.2% (100th)
Zhang et al. [20]	117.2 mAh g^{-1} 93.1%	90 mAh g^{-1} 87.8%	70 mAh g^{-1} 125.7%	
Qiu et al. [43]	110 mAh g^{-1}	90 mAh g^{-1}	66 mAh g^{-1}	50 mAh g^{-1}
Wang et al. [44]	93.5 mAh g^{-1} 91.3% (60th)			
Zhang et al. [45]	150 mAh g^{-1}	140 mAh g^{-1}	130 mAh g^{-1}	
Qu et al. [46]	140 mAh g^{-1} 98.6% (100th)	130 mAh g^{-1} 92.3% (100th)	110 mAh g^{-1} 90.9% (100th)	
Qiu et al. [47]	132.7 mAh g^{-1} 98% (500th)	118.0 mAh g^{-1} 89% (500th)	96.9 mAh g^{-1} 97% (500th)	94.5 mAh g^{-1} 91% (1000th)

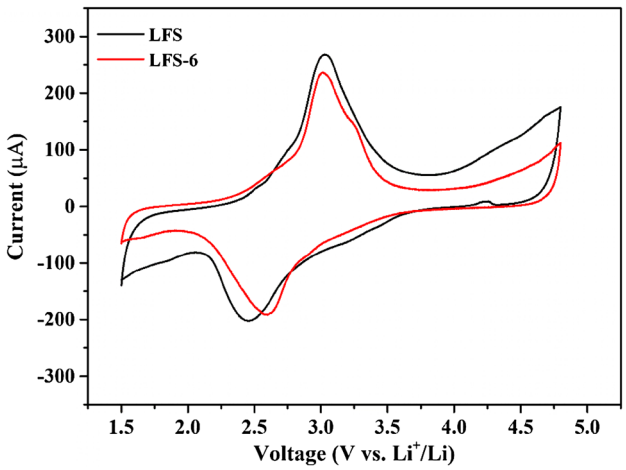

Fig. 9 Cyclic voltammetry of the composites of LFS and LFS-6 at scanning rate of 0.1 mV s^{-1}

Li_2FeSiO_4, it can enhance the cyclic stability of material to a certain degree.

In order to understand the influence of Li_3PO_4 additive on the rate performance and cyclic stability of Li_2FeSiO_4 more comprehensively, we test LFS and LFS-6 at high rate, and results are plotted in Fig. 8. For LFS-6 (Fig. 8c and d), the discharge capacities are 188.8, 172.8, 154.2 and 114.1 mAh g^{-1}, respectively, at rates of 1 C, 2 C, 5 C and 10 C. With the increasing current rate, the discharge capacities of the composite decrease gradually. After 100 cycles, the capacities are 164.9, 153.1, 152.4 and 118.9 mAh g^{-1}, respectively, with 87.3%, 88.6%, 98.8% and 104.2% of capacity attainable. In Fig. 8a and b, the discharge capacities of LFS are 177.5, 159.2, 133.0 and 89.0 mAh g^{-1}, respectively, under the same rates. After 100 cycles, the capacities declined to 129.9, 123.5, 109.1 and 75.9 mAh g^{-1}, respectively, and their corresponding capacity retentions are 73.2%, 77.6%, 82.0% and 85.3%. Additionally, our Li_2FeSiO_4 with 6 mmol% Li_3PO_4 added shows superior performances with an excellent cyclability and an outstanding rate performance than those of the previous reported Li_2FeSiO_4 summarized in Table 2.

Cyclic voltammetry (CV) was conducted to analyze the kinetic characteristics of LFS and LFS-6 composites in the second cycle, and the curves are presented in Fig. 9. From Fig. 9, it is clearly seen that the CV curves of LFS-6 are similar to that of LFS, demonstrating that Li_3PO_4 adding has no effect on the electrochemical behavior. All the electrodes exhibit a major redox couple of Fe^{2+}/Fe^{3+} at a scan rate of 0.1 mV s^{-1} in the voltage range of 1.5–4.8 V. The anodic peak at 3.04 V in LFS corresponds to the oxidation of Fe^{2+} to Fe^{3+}, and the cathodic peak at 2.45 V involving with the reduction of Fe^{3+} to Fe^{2+}, with a potential interval of 0.59 V between these two redox peaks. Compared with LFS, LFS-6 show little narrower separations of the redox peaks (a potential interval of 0.42 V), suggesting that LFS-6 has better electrochemical kinetics.

EIS measurements of LFS and LFS-6 were carried out to further study the kinetic properties of the materials. Figure 10a illustrates the Nyquist plots of the two composites and the equivalent circuit is shown inset. All the EIS spectra are divided into three characteristic regions. The semicircle at the high to medium frequency region that is assigned to the charge-transfer resistance (R_{ct}) through the solid-electrolyte interfaces, and an inclined line in the low frequency range which represents the lithium ion diffusion in the cathode material. The small intercepts by the semicircle on the real axis (Z_{re}) in the high frequency which usually correspond to the ohmic resistance of the cell (R_e), including the resistance of electrolyte, separator and electrodes. The diffusion coefficient of lithium ion (D_{Li+}) can be obtained based on the relationship between Z_{re} and the reciprocal square root of the frequency ($\omega^{-1/2}$) in the low frequency region, according to the equations mentioned [48]. From the impedance parameters

Table 3 Impedance parameters of LFS and LFS-6

	Initial				100th cycle			
	R_e (Ω)	R_{ct} (Ω)	σ (Ω cm^2 s$^{-1/2}$)	D_{Li} (cm^2 S^{-1})	R_e (Ω)	R_{ct} (Ω)	σ (Ω cm^2 s$^{-1/2}$)	D_{Li} (cm^2 S^{-1})
LFS	10.97	281.67	109.02	2.50×10^{-15}	7.80	472.99	505.26	1.17×10^{-16}
LFS-6	4.66	112.09	38.26	2.04×10^{-14}	6.58	183.43	101.39	2.91×10^{-15}

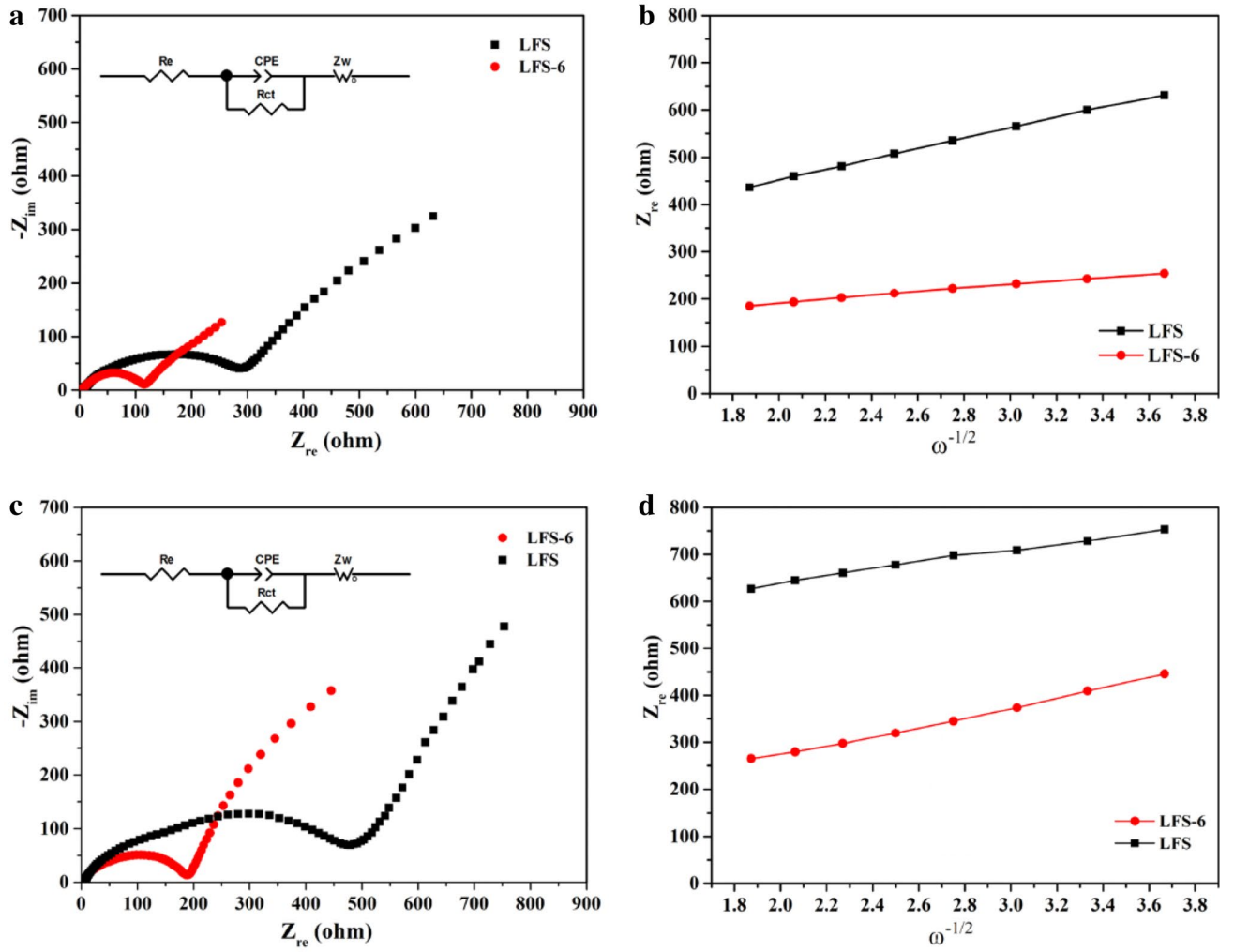

Fig. 10 The Nyquist plots and equivalent circuit of LFS and LFS-6 at room temperature (**a**, **c**) and the relationship between Z_{re} and $\omega^{-1/2}$ in the frequency region (**b**, **d**) before and after 100 cycles at 2 C rate

summarized in Table 3, it is evident that the R_{ct} value of LFS-6 (112.09 Ω) is much smaller than that of LFS (281.67 Ω) before cycling. After 100 cycles, the Rct value of LFS increased considerably in comparison with that of LFS-6. The R_{ct} of LFS increased to 472.99 Ω, but the R_{ct} of LFS-6 was 183.43 Ω. Meanwhile, the lithium ion diffusion coefficients (D_{Li}^{+}) of LFS and LFS-6 before cycling can be calculated as 2.50×10^{-15} and 2.04×10^{-14} cm^2 s^{-1}, respectively. After 100 cycles, the D_{Li+} value of LFS-6 is still higher than that of LFS. The results above clearly imply that LFS-6 shows a smaller value of charge transfer resistance with a faster diffusion coefficient. Obviously, the Li_3PO_4 adding suppress the rising of charge transfer resistance upon cycling and enhance the kinetics of lithium-ion diffusion (Fig. 10).

4 Conclusion

In summary, we synthesized and characterized Li_2FeSiO_4/Li_3PO_4/C composites, and compared their electrochemical performance with pristine one as LIB cathodes. The

$Li_2FeSiO_4/Li_3PO_4/C$ composites exhibited superior rate capability and largely improved cycling performance, especially with the amount as high as 6 mmol%. The specific discharge capacities of LFS-6 can be achieved 188.8, 172.8, 154.2 and 114.1 mAh g^{-1} at 1 C, 2 C, 5 C and 10 C, respectively, and retained 164.9, 153.1, 152.4 and 118.9 mAh g^{-1} over 100 cycles. The overall improved electrochemical performances are mainly attributed to the improved lithium ion diffusion, promoted charge transfer process and retarded side reactions by introducing lithium ion conductor Li_3PO_4. Accordingly, adding Li_3PO_4 into Li_2FeSiO_4 can be a useful way to optimize the electrochemical performance, which can also be extended to other cathodes for LIBs.

Acknowledgements This investigation is supported by National Science Foundation of China (Grant No. 21271145), the National Science Foundation of Hubei Province (Grant No. 2015CFB537) and the Science and Technology Innovation Committee of Shenzhen Municipality (contract NO. JCYJ20170306171321438).

References

1. M. Armand, J.M. Tarascon, Building better batteries. Nature **451**, 652–657 (2008)
2. J.M. Tarascon, M. Armand, Issues and challenges facing rechargeable lithium batteries. Nature **414**, 359–367 (2001)
3. G.E. Blomgren, The development and future of lithium ion batteries. J. Electrochem. Soc. **164**(1), A5019–A5025 (2017)
4. J.B. Goodenough, K.-S. Park, The Li-ion rechargeable battery: a perspective. J. Am. Chem. Soc. **135**(4), 1167–1176 (2013)
5. D. Andre, S.-J. Kim, P. Lamp, S.F. Lux, F. Maglia, O. Paschos, B. Stiaszny, Future generations of cathode materials: an automotive industry perspective. J. Mater. Chem. A **3**(13), 6709–6732 (2015)
6. J. Ni, Y. Jiang, X. Bi, L. Li, J. Lu, Lithium iron orthosilicate cathode: progress and perspectives. ACS Energy Lett. **2**(8), 1771–1781 (2017)
7. H. Wei, X. Lu, H.-C. Chiu, B. Wei, R. Gauvin, Z. Arthur, V. Emond, D.-T. Jiang, K. Zaghib, G.P. Demopoulos, Ethylenediamine-enabled sustainable synthesis of mesoporous nanostructured $Li_2Fe^{II}SiO_4$ particles from Fe(III) aqueous solution for li-ion battery application. ACS Sustain. Chem. Eng. **6**, 7458–7469 (2018)
8. R. Dominko, Li_2MSiO_4 (M = Fe and/or Mn) cathode materials. J. Power Sources **184**, 462–468 (2008)
9. A. Kokalj, R. Dominko, G. Mali, A. Meden, M. Gaberscek, K. Jamnik, Beyond one-electron reaction in Li cathode materials: designing $Li_2Mn_xFe_{1-x}SiO_4$. Chem. Mater. **19**, 3633–3640 (2007)
10. A. Liicat, J. Thomas, Li-ion migration in Li_2FeSiO_4-related cathode materials: a DFT study. Solid State Ion. **192**, 58–64 (2011)
11. L. Yi, X. Wang, G. Wang, Y. Bai, M. Liu, X. Wang, R. Yu, Improved electrochemical performance of spherical Li_2FeSiO_4/C cathode materials via Mn doping for lithium-ion batteries. Electrochim. Acta **222**, 1354–1364 (2016)
12. A. Kumar, O.D. Jayakumar, Jagannath, P. Bashiri, G.A. Nazri, V.M. Naik, R. Naik, Mg doped Li_2FeSiO_4/C nanocomposites synthesized by the solvothermal method for lithium ion batteries. Dalton Trans. **46**, 12908–12915 (2017)
13. H. Qiu, H. Yue, X. Wang, T. Zhang, M. Zhang, Z. Fang, X. Zhao, G. Chen, Y. Wei, C. Wang, D. Zhang, Titanium-doped Li_2FeSiO_4/C composite as the cathode material for lithium-ion batteries with excellent rate capability and long cycle life. J. Alloys Compd. **725**, 860–868 (2017)
14. C. Deng, S. Zhang, S.Y. Yang, B.L. Fu, L. Ma, Synthesis and characterization of $Li_2Fe_{0.97}M_{0.03}SiO_4$ ($M = Zn^{2+}$, Cu^{2+}, Ni^{2+}) cathode materials for lithium ion batteries. J. Power Sources **196**, 386–392 (2011)
15. J. Yang, X. Kang, D. He, T. Peng, L. Hu, S. Mu, Hierarchical shuttle-like Li_2FeSiO_4 as a highly efficient cathode material for lithium-ion batteries. J. Power Sources **242**, 171–178 (2013)
16. J. Yang, X. Kang, D. He, A. Zhang, M. Pan, S. Mu, Graphene activated 3D-hierarchical flower-like Li_2FeSiO_4 for high-performance lithium-ion batteries. J. Mater. Chem. A **3**, 16567–16573 (2015)
17. X. Wu, X. Wang, Y. Zhang, Nanoworm like Li_2FeSiO_4-C composites as lithium-ion battery cathodes with superior high-rate capability. ACS Appl. Mater. Interfaces. **3**, 2510–2516 (2013)
18. Y. Xu, W. Shen, A. Zhang, H. Liu, Z. Ma, Template-free hydrothermal synthesis of Li_2FeSiO_4 hollow spheres as cathode materials for lithium-ion batteries. J. Mater. Chem. A **2**, 12982–12990 (2014)
19. Z. Ding, J. Liu, J. Ran, X. Zeng, S. Yang, A. Pan, D.G. Ivey, W. Wei, Three-dimensionally ordered macroporous Li_2FeSiO_4/C composite as a high performance cathode for advanced lithium ion batteries. J. Power Sources **329**, 297–304 (2016)
20. Q. Zhang, C. Yan, Y. Meng, X. Wang, Hierarchical mesoporous Li_2FeSiO_4/C sheaf-rods as a high-performance lithium-ion battery cathode. J. Alloys Compd. **767**, 195–203 (2018)
21. Y. Fujita, T. Hira, K. Shida, M. Tsushida, J. Liao, M. Matsuda, Microstructure of high battery-performance Li_2FeSiO_4/C composite powder synthesized by combing different carbon sources in spray-freezing/freeze-drying process. Ceram. Int. **44**, 11211–11217 (2018)
22. S. Sun, C.M. Ghimbeu, C. Vis-Guterl, M.-T. Sougrati, C. Masquelier, R. Janot, Synthesis of Li_2FeSiO_4/carbon nano-composites by impregnation method. J. Power Sources **284**, 574–581 (2015)
23. X. Huang, X. Li, H. Wang, Z. Pan, M. Qu, Z. Yu, Synthesis and electrochemical performance of Li_2FeSiO_4/carbon/carbon nanotubes for lithium ion battery. Electrochim. Acta **55**, 7362–7366 (2010)
24. K.C. Kam, T. Gustafsson, J.O. Thomas, Synthesis and electrochemical properties of nanostructured Li_2FeSiO_4/C cathode. Solid State Ion. **192**, 356–359 (2011)
25. J. Bai, Z. Gong, D. Lv, Y. Li, H. Zou, Y. Yang, Nanostructured $0.8Li_2FeSiO_4/0.4Li_2SiO_3/C$ composite cathode material with enhanced electrochemical performance for lithium-ion batteries. J. Mater. Chem. **22**, 12128–12132 (2012)
26. D. Li, R. Xie, M. Tian, S. Ma, L. Gou, X. Fan, Y. Shi, H.-T.-H. Yong, L. Hao, Improving high-rate performance of mesoporous $Li_2FeSiO_4/Fe_7SiO_{10}/C$ nanocomposite cathode with a mixed valence Fe_7SiO_{10} nanocrystal. J. Mater. Chem. A **2**, 4375–4383 (2014)
27. H. Qiu, H. Yue, T. Zhang, T. Li, C. Wang, G. Chen, Y. Wei, D. Zhang, Enhanced electrochemical performance of Li_2FeSiO_4/C cathode materials by surface modification with $AlPO_4$ nanosheets. Electrochim. Acta **222**, 1870–1877 (2016)
28. K. Gaur, A.J. Pathak, H.B. Lal, Ionic and electronic conductivity in some simple lithium salts. J. Mater. Sci. **23**, 4257–4262 (1988)
29. C. Lee, P.K. Dutta, R. Ramamoorthy, S.A. Akbar, Mixed ionic and electronic conduction in Li_3PO_4 electrolyte for a CO_2 gas sensor. J. Electrochem. Soc. **153**, H4–H14 (2005)
30. C.-H. Jo, D.-H. Cho, H.-J. Noh, H. Yashiro, Y.-K. Sun, S.T. Myung, An effective method to reduce residual lithium compounds on Ni-rich $Li[Ni_{0.6}Co_{0.2}Mn_{0.2}]O_2$ active material using a

phosphoric acid derived Li_3PO_4 nanolayer. Nano Res. **8**, 1464–1479 (2015)
31. H.G. Song, J.Y. Kim, K.T. Kim, Y.J. Park, Enhanced electrochemical properties of $Li(Ni_{0.4}Co_{0.3}Mn_{0.3})O_2$ cathode by surface modification using Li_3PO_4-based materials. J. Power Sources **196**, 6847–6855 (2011)
32. Y. Jin, N. Li, C.H. Chen, S.Q. Wei, Electrochemical characterizations of commercial $LiCoO_2$ powders with surface modified by Li_3PO_4 nanoparticles. Electrochem. Solid-State Lett. **9**(6), A273–A276 (2006)
33. H. Konishi, K. Suzuki, S. Taminato, K. Kim, Y. Zheng, S. Kim, J. Lim, M. Hirayama, J.-Y. Son, Y. Cui, R. Kanno, Effect of surface Li_3PO_4 coating on $LiNi_{0.5}Mn_{1.5}O_4$ epitaxial thin film electrodes synthesized by pulsed laser deposition. J. Power Sources **269**(4), 293–298 (2014)
34. S.-X. Zhao, H. Ding, Y.-C. Wang, B.-H. Li, C.-W. Nan, Improving rate performance of $LiFePO_4$ cathode materials by hybrid coating of nano-Li_3PO_4 and carbon. J. Alloys Compd. **566**, 206–211 (2013)
35. X. Li, R. Yang, B. Cheng, Q. Hao, H. Xu, J. Yang, Y. Qian, Enhanced electrochemical properties of nano-Li_3PO_4 coated on the $LiMn_2O_4$ cathode material for lithium ion battery at 55°C. Mater. Lett. **66**, 168–171 (2012)
36. Z. Wang, S. Luo, J. Ren, D. Wang, X. Qi, Enhanced electrochemical performance of Li-rich cathode $Li[Li_{0.2}Mn_{0.54}Ni_{0.13}Co_{0.13}]O_2$ by surface modification with lithium ion conductor Li_3PO_4. Appl. Surf. Sci. **370**, 437–444 (2016)
37. X. Bian, Q. Fu, X. Bie, P. Yang, H. Qiu, Q. Pang, G. Chen, F. Du, Y. Wei, Improved electrochemical performance and thermal stability of Li-excess $Li_{1.18}Co_{0.15}Ni_{0.15}Mn_{0.52}O_2$ cathode material by Li_3PO_4 surface coating. Electrochim. Acta **174**, 875–884 (2015)
38. H. Liu, C. Chen, C. Du, X. He, G. Yin, B. Song, P. Zuo, X. Cheng, Y. Ma, Y. Gao, Lithium-rich $Li_{1.2}Ni_{0.13}Co_{0.13}Mn_{0.54}O_2$ oxide coated by Li_3PO_4 and carbon nanocomposite layers as high performance cathode materials for lithium ion batteries. J. Mater. Chem. A **3**, 2634–2641 (2015)
39. F. Wu, X. Zhang, T. Zhao, L. Li, M. Xie, R. Chen, Surface modification of cobalt-free layered $Li[Li_{0.2}Fe_{0.1}Ni_{0.15}Mn_{0.55}]O_2$ oxide with $FePO_4/Li_3PO_4$ composite as the cathode for lithium-ion batteries. J. Mater. Chem. A **3**, 9528–9537 (2015)
40. X. Wu, X. Jiang, Q. Huo, Y. Zhang, Facile synthesis of Li_2FeSiO_4/C composites with triblock copolymer P123 and their application as cathode materials for lithium ion batteries. Electrochim. Acta **80**, 50–55 (2012)
41. S.I. Nishimura, S. Hayase, R. Kanno, M. Yashima, N. Nakayama, A. Yamada, Structure of Li_2FeSiO_4. J. Am. Chem. Soc. **130**, 13212–13213 (2008)
42. A. Nyten, S. Kamali, L. Haggstrom, T. Gustafsson, J.O. Thomas, The lithium extraction/insertion mechanism in Li_2FeSiO_4. J. Mater. Chem. **16**, 2266–2272 (2006)
43. H. Qiu, K. Zhu, H. Li, T. Li, T. Zhang, H. Yue, Y. Wei, F. Du, C. Wang, G. Chen, D. Zhang, Mesoporous Li_2FeSiO_4@ordered mesoporous carbon composites cathode material for lithium-ion batteries. Carbon **87**, 365–373 (2015)
44. X. Wang, C. Qing, Q. Zhang, W. Fan, X. Huang, B. Yang, J. Cui, Facile synthesis and enhanced electrochemical performance of Li_2FeSiO_4/C/reduced graphene oxide nanocomposites. Electrochim. Acta **134**, 371–376 (2014)
45. L.-L. Zhang, S. Duan, X.-L. Yang, G. Liang, Y.-H. Huang, X.-Z. Cao, J. Yang, M. Li, M.C. Croft, C. Lewis, Insight into cobalt-doping in Li_2FeSiO_4 cathode material for lithium-ion battery. J. Power Sources **274**, 194–202 (2015)
46. L. Qu, D. Luo, S. Fang, Y. Liu, L. Yang, S. Hirano, C.-C. Yang, Mg-doped Li_2FeSiO_4/C as high-performance cathode material for lithium-ion battery. J. Power Sources **307**, 69–76 (2016)
47. H. Qiu, H. Yue, T. Zhang, Y. Ju, Y. Zhang, Z. Guo, C. Wang, G. Chen, Y. Wei, D. Zhang, Enhanced electrochemical performance of Li_2FeSiO_4/C positive electrodes for lithium-ion batteries via yttrium doping. Electrochim. Acta **188**, 636–644 (2016)
48. A.J. Bard, J.R. Faulkner, *Electrochemical methods*, 2nd edn. (Wiley, New York, 2001), p. 231